Sparse coupled logistic regression to estimate co-activation and modulatory influences of brain regions

Thomas A. W. Bolton & Dimitri Van De Ville

Chemin des Mines 09, 1202 Geneva

E-mail: `thomas.bolton@epfl.ch`

November 2019

Abstract. This abstract describes my work.
Essentially, it's awesome.
You have to accept it.

Keywords: dynamic functional connectivity, effective connectivity, logistic regression, ℓ_1 regularisation

Submitted to: *J. Neural Eng.*

1. Introduction

Understanding the structural wiring of the brain at its most global scale, and how information flows between remote processing centres, are essential questions to shed light on higher-order behaviours involving multi-modal integration and associated brain disorders. When it comes to functional magnetic resonance imaging (fMRI), the mapping of brain function is commonly performed from resting-state (RS) recordings through the computation of *functional connectivity* (FC), that is, the statistical interdependence between different time courses reflective of regional activity (Friston 1994), as can be assessed from an array of measures (Smith, Miller, Salimi-Khorshidi, Webster, Beckmann, Nichols, Ramsey & Woolrich 2010). This approach has revealed the presence of a set of RS networks (RSNs) (Damoiseaux, Rombouts, Barkhof, Scheltens, Stam, Smith & Beckmann 2006, Power, Fair, Schlaggar & Petersen 2010, Yeo, Krienen, Sepulcre, Sabuncu, Lashkari, Hollinshead, Roffman, Smoller, Zöllei, Polimeni et al. 2011), whose properties are critical landmarks of brain function and cognition (Bressler & Menon 2010, van den Heuvel & Hulshoff Pol 2010).

Over the past decade, it has become increasingly clear that quantifying FC between two brain regions as one scalar for a full scanning session is an overly simplistic approach that does not characterise the numerous reconfigurations that occur at the time scale of seconds (Chang & Glover 2010). Accordingly, many methodological pipelines have been developed to dig into time-resolved FC, and map brain function dynamically (see (Preti, Bolton & Van De Ville 2017, Lurie, Kessler, Bassett, Betzel, Breakspear, Keilholz, Kucyi, Liégeois, Lindquist & McIntosh 2018) for contemporary reviews).

The most notorious family of dynamic approaches simplifies the originally voxel-wise fMRI data into a state-level representation: first, FC is computed over successive temporal sub-windows, and the concatenated data across the full subject population at hand is subjected to hard clustering to yield a set of dynamic FC (dFC) states (Allen, Damaraju, Plis, Erhardt, Eichele & Calhoun 2014, Damaraju, Allen, Belger, Ford, McEwen, Mathalon, Mueller, Pearlson, Potkin, Preda, Turner, Vaidya, van Erp & Calhoun 2014). Because spatial Independent Component Analysis (ICA) is typically performed prior to clustering, each state stands for a set of RSNs showing specific correlational relationships.

In other analytical schemes, whole-brain voxelwise activity (Liu, Chang & Duyn 2013), or activity transients (Karahanoğlu & Van De Ville 2015), undergo clustering instead of FC patterns; in this case, each of the retrieved centroids directly stands for an RSN. If temporal ICA is applied after spatial ICA, temporally mutually independent RSNs are retrieved (Smith, Miller, Moeller, Xu, Auerbach, Woolrich, Beckmann, Jenkinson, Andersson, Glasser et al. 2012). Finally, the use of a hidden Markov model (HMM) also enables to derive RSNs, as represented under the form of (sparse) FC patterns (Eavani, Satterthwaite, Gur, Gur & Davatzikos 2013, Vidaurre, Smith & Woolrich 2017) or

vectors of activation (Chen, Langely, Chen & Hu 2016).

In all the above cases, there is the underlying assumption that the raw fMRI data can be downscaled to a set of RSNs, and that the dynamics of brain function should be understood from this simplified starting point. Recent results, however, question the validity of this assumption: for instance, some brain regions do not remain attached to the same network throughout a scanning session, but instead adjust their modular allegiance over time in a way that relates to cognitive performance (Chen, Cai, Ryali, Supekar & Menon 2016, Pedersen, Zalesky, Omidvarnia & Jackson 2018). In addition, brain regions or networks also morph spatially over time (Kiviniemi, Vire, Remes, Elseoud, Starck, Tervonen & Nikkinen 2011, Kottaram, Johnston, Ganella, Pantelis, Kotagiri & Zalesky 2018, Iraji, Fu, Damaraju, DeRamus, Lewis, Bustillo, Lenroot, Belger, Ford, McEwen et al. 2019).

To capture these spatially more subtle reconfigurations, novel methodologies have attempted to operate at the regional scale, and the assessment of *causal* relationships (*i.e.*, from time t to $t + 1$) between distinct areas showed particular merits as an alternative conceptualisation of RS functional brain dynamics, be it through autoregressive models (Liégeois, Laumann, Snyder, Zhou & Yeo 2017, Lennartz, Schiefer, Rotter, Hennig & LeVan 2018) or Ornstein-Uhlenbeck processes (Gilson, Moreno-Bote, Ponce-Alvarez, Ritter & Deco 2016).

At present, there are thus two conceptually discrepant ways to view RS dFC: on the one hand, expressing it as sets of simultaneously activating regions that make networks, and on the other hand, viewing it as effective connectivity between individual areas. It remains to be determined which of these two viewpoints offers the best representation of RS dynamics, and whether they describe overlapping or distinct facets of the data.

In this work, we have attempted to progress in answering these questions by developing a novel methodological framework that jointly estimate sets of co-activations, and causal couplings, between individual brain regions. A dedicated parameter also enables to modulate the trade-off in data fitting between these two viewpoints.

2. Materials and Methods

2.1. Mathematical framework

Let us denote the activity of a region r (out of R in total) at time t as $h_t^{(r)}$. We hypothesise two possible states of activity: *baseline* ($h_t^{(r)} = 0$) or *active* ($h_t^{(r)} = +1$). Each region may interact with all the other areas $s \neq r$ in two ways: (1) showing simultaneous activity (that is, episodes of co-activation), or (2) being causally modulated. To jointly describe these two phenomena, we characterise the probability of a region r to switch between activity states as a logistic regression (Friedman, Hastie & Tibshirani 2010):

$$\begin{cases} \mathcal{P}(h_{t+1}^{(r)} = +1 | h_t^{(r)} = 0, \mathbf{h}_t^{(-\mathbf{r})}, \mathbf{h}_{t+1}^{(-\mathbf{r})}) = \frac{1}{1+e^{-(\alpha_A^{(r)} + \boldsymbol{\gamma}_A^{(r)\top} \mathbf{h}_{t+1}^{(-\mathbf{r})} + \boldsymbol{\beta}_A^{(r)\top} \mathbf{h}_t^{(-\mathbf{r})})}} \\ \mathcal{P}(h_{t+1}^{(r)} = 0 | h_t^{(r)} = +1, \mathbf{h}_t^{(-\mathbf{r})}, \mathbf{h}_{t+1}^{(-\mathbf{r})}) = \frac{1}{1+e^{-(\alpha_D^{(r)} + \boldsymbol{\gamma}_D^{(r)\top} \mathbf{h}_{t+1}^{(-\mathbf{r})} + \boldsymbol{\beta}_D^{(r)\top} \mathbf{h}_t^{(-\mathbf{r})})}} \end{cases} . \quad (1)$$

The baseline-to-active transition is modelled by the first equation, while the return to baseline from an active state is governed by the second. Associated coefficients are respectively written with the $\cdot_A$ and $\cdot_D$ subscripts. In what follows, for the sake of clarity, we will omit these subscripts and only show one set of equations, as the formulations are strictly equivalent for both types of transitions.

If all other regions are at a baseline level of activity at the start ($\mathbf{h}_t^{(-\mathbf{r})} = \mathbf{0}$) and end ($\mathbf{h}_{t+1}^{(-\mathbf{r})} = \mathbf{0}$) of the transition, only the scalar coefficient $\alpha^{(r)}$ plays a role in shaping the transition likelihood. The vector $\boldsymbol{\gamma}^{(r)} \in \mathbb{R}^{R-1}$ contains the co-activation coefficients for all regions $s \neq r$: positive-valued coefficients will enhance the likelihood of the transition of interest if $h_{t+1}^{(s)} = +1$ (that is, if regions r and s are co-active at time $t+1$). Negative-valued coefficients will, likewise, reduce the transition probability. The reasoning is similar for the vector $\boldsymbol{\beta}^{(r)} \in \mathbb{R}^{R-1}$, except that a modulatory effect is then exerted if $h_t^{(s)} = +1$ (*i.e.*, region s is active before the transition, resulting in a causal modulation instead of a co-activation).

If the above pair of equations is considered for each brain region, the resulting coefficients can be arranged in two types of matrices, where the rth column contains the influences onto region r (diagonal elements are left empty): one type is reflective of co-activations, which we be termed $\boldsymbol{\Gamma}$, and one symbolises causal modulations, and will be referred to as $\mathbf{B}$. $\boldsymbol{\Gamma}$ and $\mathbf{B}$ can respectively be interpreted as equivalents of the functional connectome and effective connectome.

The concomitant modelling of co-activations and causal modulations enables to jointly derive the two sets of coefficients. Given the fact that the resting brain is often described as a series of RSNs (Damoiseaux et al. 2006, Power et al. 2010, Yeo et al. 2011), we expect $\boldsymbol{\Gamma}$ to only contain a sparse subset of non-null entries. Similarly, only a restricted amount of areas or networks are expected to causally modulate each other (Christoff,

Irving, Fox, Spreng & Andrews-Hanna 2016, Bolton, Tarun, Sterpenich, Schwartz & Van De Ville 2017). To fit these neurobiological priors, while also enabling convergence of the framework with fewer data points, we appended an ℓ_1 regularisation term:

$$\xi||\boldsymbol{\gamma}^{(r)}||_1 + (1-\xi)||\boldsymbol{\beta}^{(r)}||_1 < \rho \quad \forall \quad r = 1, ..., R. \tag{2}$$

In the above, the parameter ρ controls the extent of regularisation casted on all coefficients (it is associated to an inversely proportional parameter λ in the optimisation equation detailed below). The parameter ξ enables to balance the extent with which the co-activation and causal sets are regularised: if $\xi = 0$, regularisation only operates on causal coefficients, while if $\xi = 1$, only co-activation coefficients are made sparse. This respectively amounts to a description of regional brain dynamics where co-activations, or causal influences, dominate.

2.2. Implementation

Solving the above set of coupled logistic regression equations requires that the activity levels of all regions be known. To binarise the input time courses, we individually z-score each, and set to 1/0 the time points with a value above/below 0. While binarisation may remove part of the insightful information from the original data, it has been used in recently developed methodological pipelines (Kang, Pae & Park 2019). In the discussion, we touch upon possibilities to make the framework amenable to a case with more than 2 states of activity.

After defining the activation states, initial parameter estimates can be computed. Co-activation and modulatory coefficients are all set to 0, and intrinsic transition probabilities are estimated by a standard HMM approach (Rabiner 1989).

Following (Friedman et al. 2010), in a regularised logistic regression, one attempts to solve the following:

$$\min_{\alpha^{(r)},\boldsymbol{\gamma}^{(r)},\boldsymbol{\beta}^{(r)}} -\mathcal{L}^{(r)}(\alpha^{(r)}, \boldsymbol{\gamma}^{(r)}, \boldsymbol{\beta}^{(r)}) + \lambda(\xi||\boldsymbol{\gamma}^{(r)}||_1 + (1-\xi)||\boldsymbol{\beta}^{(r)}||_1), \tag{3}$$

where r is the assessed region, and the log-likelihood is approximated as:

$$\mathcal{L}^{(r)}(\alpha^{(r)}, \boldsymbol{\gamma}^{(r)}, \boldsymbol{\beta}^{(r)}) = -\frac{1}{2|\mathcal{T}|}\sum_{t\in\mathcal{T}} \omega_t(z_t - \alpha^{(r)} - \boldsymbol{\gamma}^{(r)\top}\mathbf{h}_{t+1}^{(-\mathbf{r})} - \boldsymbol{\beta}^{(r)\top}\mathbf{h}_t^{(-\mathbf{r})}) + C. \tag{4}$$

The ensemble $\mathcal{T}$ contains all the data points for which the probed region is in the start state of interest at time t (*e.g.*, baseline for the baseline-to-active transitions), and C is a constant. If we denote the probability of the transition of interest as $p(\alpha^{(r)}, \boldsymbol{\gamma}^{(r)}, \boldsymbol{\beta}^{(r)}, \mathbf{h}_t^{(-\mathbf{r})}, \mathbf{h}_{t+1}^{(-\mathbf{r})})$, the parameters ω_t and z_t depend on the current estimates

of the coefficients—which we denote with a tilda—as:

$$\begin{cases} \omega_t = p(\tilde{\alpha}^{(r)}, \tilde{\boldsymbol{\gamma}}^{(r)}, \tilde{\boldsymbol{\beta}}^{(r)}, \mathbf{h}_t^{(-\mathbf{r})}, \mathbf{h}_{t+1}^{(-\mathbf{r})}) - p(\tilde{\alpha}^{(r)}, \tilde{\boldsymbol{\gamma}}^{(r)}, \tilde{\boldsymbol{\beta}}^{(r)}, \mathbf{h}_t^{(-\mathbf{r})}, \mathbf{h}_{t+1}^{(-\mathbf{r})})^2 \\ z_t = \tilde{\alpha}^{(r)} + \tilde{\boldsymbol{\gamma}}^{(r)\top} \mathbf{h}_{t+1}^{(-\mathbf{r})} + \tilde{\boldsymbol{\beta}}^{(r)\top} \mathbf{h}_t^{(-\mathbf{r})} + \frac{y_t - p(\tilde{\alpha}^{(r)}, \tilde{\boldsymbol{\gamma}}^{(r)}, \tilde{\boldsymbol{\beta}}^{(r)}, \mathbf{h}_t^{(-\mathbf{r})}, \mathbf{h}_{t+1}^{(-\mathbf{r})})}{\omega_t} \end{cases} . \quad (5)$$

y_t defines whether there was a change in activity level from time t to $t+1$ or not (respectively, $y_t = 1$ or $y_t = 0$). Coefficients are iteratively estimated by a coordinate-wise descent algorithm, following (Friedman, Hastie, Höfling, Tibshirani et al. 2007): the initial estimates outlined above are used at the maximal regularisation level λ_{MAX}, and individual coefficients are successively re-estimated in random order (note that for $\alpha^{(r)}$ coefficients, which do not enter the ℓ_1 regularisation term, soft shrinkage is not required). The process continues until the change across two iterations becomes lower than a defined tolerance threshold ϵ. The next regularisation level is then considered, using warm restarts to speed up computations (*i.e.*, the estimates obtained at the end of a regularisation cycle are used as initial values for the following one).

In all the analyses performed in this work, we considered a regularisation path with $\lambda \in [10000, 0.02]$ (206 logarithmically distributed values), compared five levels of trade-off between co-activation and causal coefficients ($\xi = \{0, 0.25, 0.5, 0.75, 1\}$), and used a tolerance $\epsilon = 10^{-40}$.

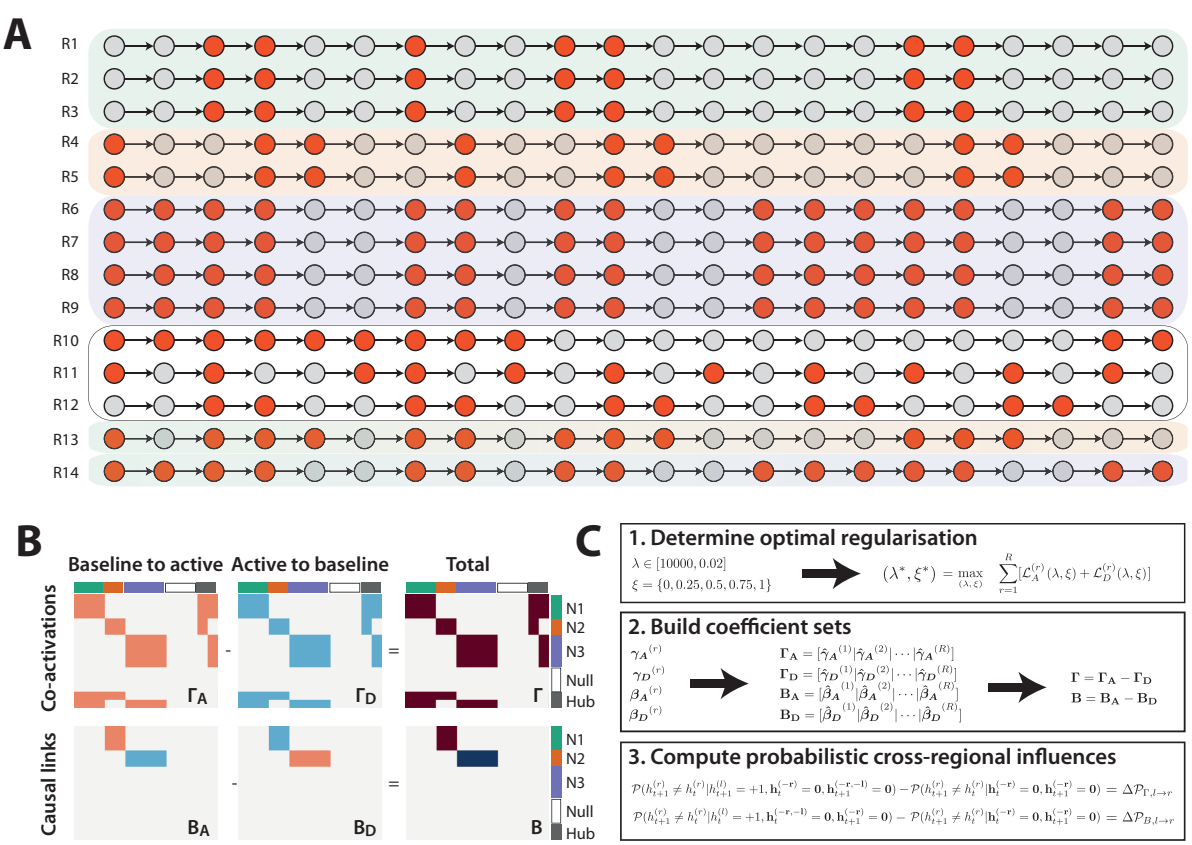

Figure 1. Overview of the framework. (A) AAA.

2.3. Simulated data

We first sought to validate our pipeline on simulated data examples containing cross-regional causal modulations as well as co-activations. To do so, we considered parameters resembling those of the assessed experimental data (see the following section) as much as possible. We thus considered simulated activity time courses for $R = 45$ regions, for a total of $S = 135$ subjects and $T = 1190$ time points per subject.

In light of the RS literature (Yeo et al. 2011), in our main simulations, we considered the presence of $N = 7$ separate RSNs (we also assessed a more finely segmented case with $N = 17$; see Supplementary Figure 1). We included three different types of regions:

- Regions belonging to one of the N networks
- Regions evolving with their own, independent dynamics (which can be regarded as *null* cases)
- Regions that jointly belong to more than one network (that is, *hubs*)

Blabla

2.4. Experimental fMRI data

We applied our framework to experimental fMRI data from the *Human Connectome Project*.

3. Results

4. Discussion

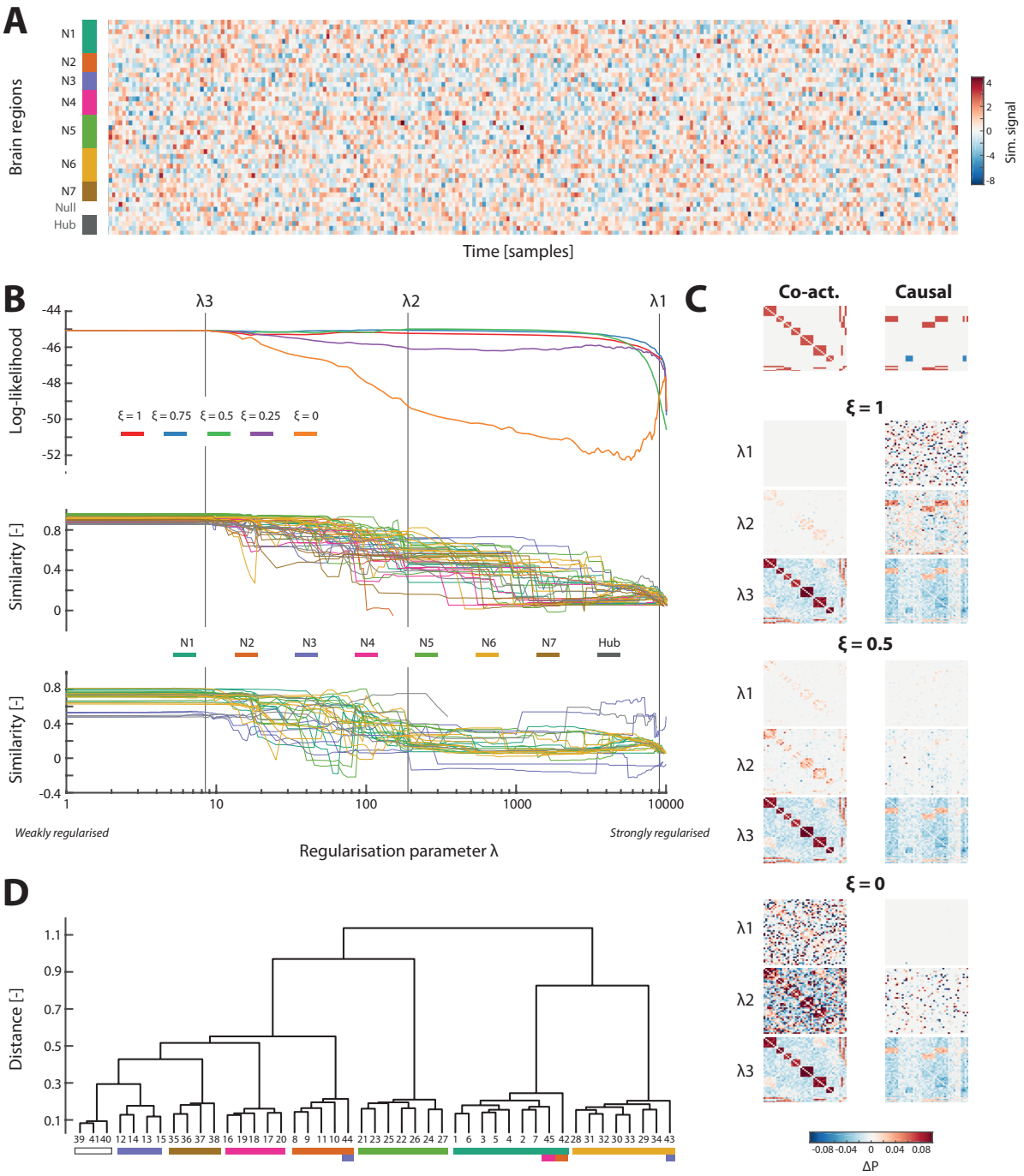

Figure 2. Results on simulated data. (A) AAA.

Allen, E. A., Damaraju, E., Plis, S. M., Erhardt, E. B., Eichele, T. & Calhoun, V. D. (2014). Tracking whole-brain connectivity dynamics in the resting state, *Cerebral Cortex* **24**(3): 663–676.

Bolton, T. A. W., Tarun, A., Sterpenich, V., Schwartz, S. & Van De Ville, D. (2017). Interactions between large-scale functional brain networks are captured by sparse coupled hmms, *IEEE Transactions on Medical Imaging* **37**(1): 230–240.

Bressler, S. L. & Menon, V. (2010). Large-scale brain networks in cognition: emerging methods and principles, *Trends in Cognitive Sciences* **14**(6): 277–290.

Chang, C. & Glover, G. H. (2010). Time-frequency dynamics of resting-state brain connectivity measured with fMRI, *Neuroimage* **50**(1): 81–98.
URL: *http://dx.doi.org/10.1016/j.neuroimage.2009.12.011*

Chen, S., Langely, J., Chen, X. & Hu, X. (2016). Spatiotemporal modeling of brain dynamics using resting-state functional magnetic resonance imaging with Gaussian hidden Markov model, *Brain Topography* **6**(4): 326–334.

Chen, T., Cai, W., Ryali, S., Supekar, K. & Menon, V. (2016). Distinct global brain dynamics and spatiotemporal organization of the salience network, *PLOS Biology* **14**(6): 1–21.
URL: *https://journals.plos.org/plosbiology/article/file?id=10.1371/journal.pbio.1002469&type=printable*

Christoff, K., Irving, Z. C., Fox, K. C. R., Spreng, R. N. & Andrews-Hanna, J. R. (2016). Mind-wandering as spontaneous thought: a dynamic framework, *Nature Reviews Neuroscience* **17**(11): 718–731.
URL: *http://www.nature.com/doifinder/10.1038/nrn.2016.113*

Damaraju, E., Allen, E. A., Belger, A., Ford, J. M., McEwen, S., Mathalon, D. H., Mueller, B. A., Pearlson, G. D., Potkin, S. G., Preda, A., Turner, J. A., Vaidya, J. G., van Erp, T. G. & Calhoun, V. D. (2014). Dynamic functional connectivity analysis reveals transient states of dysconnectivity in schizophrenia, *Neuroimage: Clinical* **5**: 298–308.
URL: *http://dx.doi.org/10.1016/j.nicl.2014.07.003 http://linkinghub.elsevier.com/retrieve/pii/S2213158214000953*

Damoiseaux, J. S., Rombouts, S. A. R., Barkhof, F., Scheltens, P., Stam, C. J., Smith, S. M. & Beckmann, C. F. (2006). Consistent resting-state networks across healthy subjects, *Proceedings of the National Academy of Sciences* **103**(37): 13848–13853.
URL: *http://www.pnas.org/content/103/37/13848.short*

Eavani, H., Satterthwaite, T. D., Gur, R. E., Gur, R. C. & Davatzikos, C. (2013). Unsupervised learning of functional network dynamics in resting state fMRI, *Lecture Notes in Computer Science* **7917**: 426–437.
URL: *https://www.ncbi.nlm.nih.gov/pmc/articles/PMC3974209/pdf/nihms-504470.pdf*

Friedman, J., Hastie, T., Höfling, H., Tibshirani, R. et al. (2007). Pathwise coordinate optimization, *The Annals of Applied Statistics* **1**(2): 302–332.

Friedman, J., Hastie, T. & Tibshirani, R. (2010). Regularization paths for generalized linear models via coordinate descent, *Journal of Statistical Software* **33**(1): 1.

Friston, K. J. (1994). Functional and effective connectivity in neuroimaging: A synthesis, *Human Brain Mapping* **2**(1): 56–78.

Gilson, M., Moreno-Bote, R., Ponce-Alvarez, A., Ritter, P. & Deco, G. (2016). Estimation of directed effective connectivity from fmri functional connectivity hints at asymmetries of cortical connectome, *PLOS Computational Biology* **12**(3): e1004762.

Iraji, A., Fu, Z., Damaraju, E., DeRamus, T. P., Lewis, N., Bustillo, J. R., Lenroot, R. K., Belger, A., Ford, J. M., McEwen, S. et al. (2019). Spatial dynamics within and between brain functional domains: A hierarchical approach to study time-varying brain function, *Human Brain Mapping* **40**(6): 1969–1986.

Kang, J., Pae, C. & Park, H. (2019). Graph-theoretical analysis for energy landscape reveals the organization of state transitions in the resting-state human cerebral cortex, *PLOS ONE* **14**(9): 0222161.

Karahanoğlu, F. I. & Van De Ville, D. (2015). Transient brain activity disentangles fMRI resting-state dynamics in terms of spatially and temporally overlapping networks, *Nature Communications*

6: 7751.
URL: *http://www.nature.com/doifinder/10.1038/ncomms8751*

Kiviniemi, V., Vire, T., Remes, J., Elseoud, A. A., Starck, T., Tervonen, O. & Nikkinen, J. (2011). A sliding time-window ICA reveals spatial variability of the default mode network in time, *Brain Connectivity* **1**(4): 339–347.
URL: *http://www.liebertonline.com/doi/abs/10.1089/brain.2011.0036*

Kottaram, A., Johnston, L., Ganella, E., Pantelis, C., Kotagiri, R. & Zalesky, A. (2018). Spatio-temporal dynamics of resting-state brain networks improve single-subject prediction of schizophrenia diagnosis, *Human Brain Mapping* **39**(9): 3663–3681.

Lennartz, C., Schiefer, J., Rotter, S., Hennig, J. & LeVan, P. (2018). Sparse estimation of resting-state effective connectivity from fmri cross-spectra, *Frontiers in Neuroscience* **12**: 287.

Liégeois, R., Laumann, T. O., Snyder, A. Z., Zhou, J. & Yeo, B. T. T. (2017). Interpreting temporal fluctuations in resting-state functional connectivity mri, *Neuroimage* **163**: 437–455.

Liu, X., Chang, C. & Duyn, J. H. (2013). Decomposition of spontaneous brain activity into distinct fMRI co-activation patterns, *Frontiers in Systems Neuroscience* **7**: 1–11.
URL: *http://journal.frontiersin.org/article/10.3389/fnsys.2013.00101/abstract*

Lurie, D., Kessler, D., Bassett, D., Betzel, R. F., Breakspear, M., Keilholz, S., Kucyi, A., Liégeois, R., Lindquist, M. A. & McIntosh, A. R. (2018). On the nature of resting fmri and time-varying functional connectivity, *PsyArXiv* .

Pedersen, M., Zalesky, A., Omidvarnia, A. & Jackson, G. D. (2018). Multilayer network switching rate predicts brain performance, *Proceedings of the National Academy of Sciences* **115**(52): 13376–13381.

Power, J. D., Fair, D. A., Schlaggar, B. L. & Petersen, S. E. (2010). The Development of Human Functional Brain Networks, *Neuron* **67**(5): 735–748.
URL: *http://dx.doi.org/10.1016/j.neuron.2010.08.017 http://ac.els-cdn.com/S0896627310006276/1-s2.0-S0896627310006276-main.pdf?_tid=530b28c0-358b-11e7-8056-00000aacb35d&acdnat=1494425996_7e5fc23be3ab984395a36c2a6fa42bfb*

Preti, M. G., Bolton, T. A. W. & Van De Ville, D. (2017). The dynamic functional connectome: State-of-the-art and perspectives, *Neuroimage* **160**: 41–54.
URL: *https://ac.els-cdn.com/S1053811916307881/1-s2.0-S1053811916307881-main.pdf?_tid=740fef8f-835b-4993-86d3-a6f60b841679&acdnat=1523360042_29ea611d8892cbd9e44c8ac92ff16e62*

Rabiner, L. R. (1989). A tutorial on hidden markov models and selected applications in speech recognition, *Proceedings of the IEEE* **77**(2): 257–286.

Smith, S. M., Miller, K. L., Moeller, S., Xu, J., Auerbach, E. J., Woolrich, M. W., Beckmann, C. F., Jenkinson, M., Andersson, J., Glasser, M. F. et al. (2012). Temporally-independent functional modes of spontaneous brain activity, *Proceedings of the National Academy of Sciences* **109**(8): 3131–3136.

Smith, S. M., Miller, K. L., Salimi-Khorshidi, G., Webster, M., Beckmann, C. F., Nichols, T. E., Ramsey, J. D. & Woolrich, M. W. (2010). Network modelling methods for fMRI, *NeuroImage* .

van den Heuvel, M. P. & Hulshoff Pol, H. E. (2010). Exploring the brain network: A review on resting-state fMRI functional connectivity, *European Neuropsychopharmacology* **20**(8): 519–534.

Vidaurre, D., Smith, S. M. & Woolrich, M. W. (2017). Brain network dynamics are hierarchically organized in time, *Proceedings of the National Academy of Sciences* **114**(48): 201705120.
URL: *http://www.pnas.org/lookup/doi/10.1073/pnas.1705120114*

Yeo, B. T. T., Krienen, F. M., Sepulcre, J., Sabuncu, M. R., Lashkari, D., Hollinshead, M., Roffman, J. L., Smoller, J. W., Zöllei, L., Polimeni, J. R. et al. (2011). The organization of the human cerebral cortex estimated by intrinsic functional connectivity, *Journal of Neurophysiology* **106**(3): 1125–1165.